Inorganic Chemistry

ARTICLE

pubs.acs.org/IC

Phosphorescence vs Fluorescence in Cyclometalated Platinum(II) and Iridium(III) Complexes of (Oligo)thienylpyridines

Dmitry N. Kozhevnikov,*[,†,‡] Valery N. Kozhevnikov,[§] Marsel Z. Shafikov,[‡] Anton M. Prokhorov,[‡,∥] Duncan W. Bruce,*[,∥] and J. A. Gareth Williams*[,⊥]

[†]I. Postovsky Institute of Organic Synthesis, Ekaterinburg, 620041, Russia

[‡]Ural Federal University, Mira 19, Ekaterinburg, 620002, Russia

[§]School of Life Sciences, Northumbria University, Newcastle-Upon-Tyne, Ne1 8st, United Kingdom

[∥]Department of Chemistry, University of York, Heslington, York, Yo10 5dd, United Kingdom

[⊥]Department of Chemistry, Durham University, South Road, Durham, Dh1 3le, United Kingdom

Supporting Information

ABSTRACT: Two newly prepared oligothienylpyridines, 5-(2-pyridyl)-5′-dodecyl-2,2′-bithiophene, **HL**^{2}, and 5-(2-pyridyl)-5″-dodecyl-2,2′:5′,2″-ter-thiophene, **HL**^{3}, bind to platinum(II) and iridium(III) as *N*∧*C*-coordinating ligands, cyclometallating at position C^4 in the thiophene ring adjacent to the pyridine, leaving a chain of either one or two pendent thiophenes. The synthesis of complexes of the form [PtL^n(acac)] and [Ir(L^n)$_2$(acac)] (n = 2 or 3) is described. The absorption and luminescence properties of these four new complexes are compared with the behavior of the known complexes [PtL^1(acac)] and [Ir(L^1)$_2$(acac)] {HL^1 = 2-(2-thienyl)pyridine}, and the profound differences in behavior are interpreted with the aid of time-dependent density functional theory (TD-DFT) calculations. Whereas [PtL^1(acac)] displays solely intense phosphorescence from a triplet state of mixed $\pi\pi^*$/MLCT character, the phosphorescence of [PtL^2(acac)] and [PtL^3(acac)] is weak, strongly red shifted, and accompanied by higher-energy fluorescence. TD-DFT reveals that this difference is probably due to the metal character in the lowest-energy excited states being strongly attenuated upon introduction of the additional thienyl rings, such that the spin−orbit coupling effect of the metal in promoting intersystem crossing is reduced. A similar pattern of behavior is observed for the iridium complexes, except that the changeover to dual emission is delayed to the terthiophene complex [Ir(L^3)$_2$(acac)], reflecting the higher degree of metal character in the frontier orbitals of the iridium complexes than their platinum counterparts.

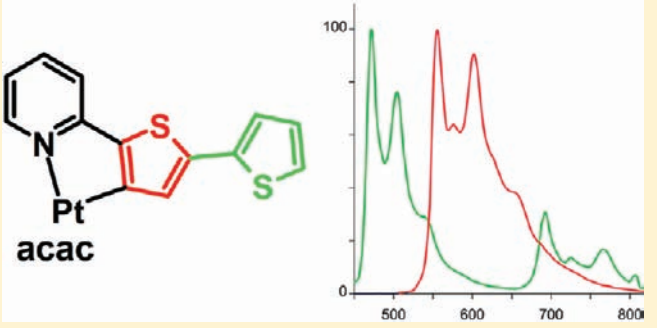

INTRODUCTION

Complexes of iridium(III) and platinum(II) with heterocyclic ligands, such as polypyridines and their cyclometallating aryl analogues, have found a wide range of applications in the context of photoactive molecular materials.[1,2] These include photocatalysts,[3] photochemical solar energy conversion,[4] biological labels,[5] and, in particular, phosphorescent dopants in the electroluminescent layers of organic light-emitting diodes (OLEDs).[6] The high spin−orbit coupling (SOC) associated with the heavy metal atom can promote the triplet → singlet radiative transition, so that such complexes may exhibit unusually high phosphorescence quantum yields at room temperature and relatively short triplet emission decay times.[7] In addition, intersystem crossing (ISC) from the singlet (S_1) to the triplet state (typically T_1) is also accelerated and normally depopulates the former at a rate (10^{12} s^{-1}) much faster than that of radiative emission from the singlet state (10^8−10^9 s^{-1}).[8] As a result, fluorescence is not commonly observed from discrete complexes of the third-row transition-metal complexes, although a few examples are known, for example, where a ligand incorporates a π-conjugated chromophoric ligand somewhat remote from the metal center.[9]

In order for the metal ion to exert the above SOC effects and promote phosphorescence, its orbitals should make a significant contribution to the frontier orbitals involved in the excited states. For larger complexes with more extended ligands or in which there is a saturated linker between the metal-containing moiety and that part of the molecule on which the excited state is primarily localized, the influence of the metal is expected to be attenuated. Typically, this may lead to longer triplet radiative lifetimes, as the excited state becomes more like a purely organic

Received: January 31, 2011
Published: March 23, 2011

one, although the rate of S → T ISC may still be sufficient to eliminate fluorescence. Elongation of the luminescence lifetimes of iridium terpyridyl complexes upon going from phenyl to biphenyl substituents is an example of such a case.[10] Meanwhile, Chi and Chou and co-workers made a detailed study of dual emission in a series of osmium complexes, in which the proportion of fluorescence to phosphorescence varied according to the identity of a π-conjugated aromatic system appended to a β-diketonate ligand.[11] Key points relating to the attenuation of SOC in such complexes have been reviewed recently.[11b] There are also some cases of Pt(II) complexes, particularly those in which the ligands have been appended with additional moieties favoring, for example, charge-transport properties for use in OLEDs, which show dual luminescence (typically dominant fluorescence from a remote organic substituent and minor phosphorescence related with the metal and ligating unit).[12]

Cyclometalated iridium(III) and platinum(II) complexes of arylpyridines are well known to be often strongly phosphorescent at room temperature.[13−15] Chemical modification of the chromophoric cyclometallating ligand enables tuning of the emitting properties in a manner that can be readily understood in terms of the influence of electron-donating and -withdrawing substituents on the energies of the frontier orbitals.[16] Iridium complexes of such ligands, in particular, have attracted a great deal of interest as OLED phophors, for example, $[Ir(ppy)_3]$, $[Ir(F_2ppy)_2(pic)]$, and $[Ir(piq)_2(acac)]$ as green, blue, and red emitters, respectively {ppyH = 2-phenylpyridine; F_2ppyH = 2-(2,4-difluorophenyl)pyridine; piqH = 1-phenylisoquinoline; picH = picolinic acid; acacH = 2,4-pentanedione}.[17−19] Thienylpyridines, in which the phenyl group has been replaced by a thiophene ring, are also potentially interesting ligands for generating luminescent complexes. The more electron-rich nature of the thiophene ring compared to the benzene ring is known to lead to red shifts in the emission energy of thienylpyridine complexes compared to those of ppy, an effect attributed primarily to destabilization of the highest occupied orbitals {thpy =2-(2-thienyl)pyridine}.

Meanwhile, oligo- and polythiophenes, long a source of fascination for the conducting properties that arise upon doping them with electrons or holes,[20] are also of interest for their fluorescence properties. Typically, they have high quantum yields of fluorescence, with emission energies that are influenced sensitively by molecular and environmental factors, properties that have been exploited in fluorescent sensory systems, among others.[21]

The combination of these two types of molecular units, namely, an oligothiophene and a cyclometalated thienylpyridine, should thus be an intriguing system to consider and is the subject of the current paper. We describe the synthesis and photophysical properties of cyclometalated Pt(II) and Ir(III) complexes of 2-(oligothienyl)pyridines. The molecules are derivatives of the known compounds $[PtL^1(acac)]$ and $[Ir(L^1)_2(acac)]$, where HL^1 = 2-(2-thienyl)pyridine (here studied as models), carrying either one or two additional thiophene rings on the metalated thienyl ring. One might reason that the metal ion would promote formation of the triplet state of the oligothiophene, leading to efficient low-energy phosphorescence, or that the extended nature of the ligand might attentuate the effect of the metal, such that formation of the triplet state would become inefficient and fluorescence might compete effectively. We show that the extension of the ligand does dramatically alter the emission properties, fluorescence is indeed observed, but nonradiative decay pathways unexpectedly limit efficiencies severely compared both to the fluorescence of oligothiophenes and to the phosphorescence of the parent, unsubstituted cyclometalated complexes. The results are interpreted with the aid of calculations using time-dependent density functional theory (TD-DFT).

RESULTS AND DISCUSSION

1. Synthesis of Ligands and Complexes. New proligands—pyridines with bi- or terthiophene chains at position 2—were synthesized by the Stille couplings of appropriate bromothienylpyridines and 2-(tributyltin)thiophene. A dodecyl chain was incorporated into the ligands in order to increase their solubility and, especially, the solubility of the ensuing complexes. The reaction of 2-(2-bromothien-5-yl)pyridine, **1**, with 2-(tributyltin)-5-dodecylthiophene, **2**, in the presence of tetrakis-(triphenylphosphine) palladium(0) as catalyst gave proligand $\mathbf{HL^2}$ bearing a bithiophene moiety (Scheme 1). The same reaction of **1** with 2-(tributyltin) thiophene, **3**, followed by bromination of the resulting bithienylpyridine, **4**, gave the halogen precursor **5**. Finally, the cross-coupling reaction of **5** with **2** gave the terthienylpyridine proligand $\mathbf{HL^3}$.

Platinum complexes incorporating the new ligands $\mathbf{L^2}$ and $\mathbf{L^3}$ coordinated to the metal in a cyclometalated $N\wedge C^{3\prime}$ fashion, $[PtL^n(acac)]$, were obtained through the intermediacy of the dichloro-bridged dimer complexes $[PtL^n(\mu\text{-Cl})]_2$ and their reaction with sodium acetylacetonate in acetone in a modification to the previously described procedure for $[Pt(ppy)(acac)]$[14] (Scheme 2). The corresponding cyclometalated iridium complexes $[Ir(L^n)_2(acac)]$ were obtained in a one-pot procedure upon reaction of the proligands $\mathbf{HL^2}$ and $\mathbf{HL^3}$ with $IrCl_3 \cdot xH_2O$ and sodium acetylacetonate in ethoxyethanol under reflux (Scheme 2). In the sections which follow, the platinum(II) and iridium(III) complexes of $\mathbf{L^1}$, $\mathbf{L^2}$, and $\mathbf{L^3}$ will be abbreviated **Pt-1**, **Pt-2**, and **Pt-3** and **Ir-1**, **Ir-2**, and **Ir-3,** respectively (Figure 1).

2. UV−Visible Absorption and Emission Spectroscopy of the Proligands HL^1 − HL^3. The absorption spectra of the proligands are shown in Figure 2, and numerical absorption and emission data for all compounds are summarized in Table 1. The extension from one to two to three thiophenes leads to a progressive shift in the lowest-energy absorption band to longer wavelengths, as typically observed for polyaryls. Introduction of the second thiophene unit stabilizes the excited state by 5500 cm^{-1}, while the third leads to a smaller decrease of 2500 cm^{-1}. This red shift is accompanied by a substantial increase in the extinction coefficient.

All three compounds are fluorescent in solution at room temperature (Figure 3 and Table 1). The emission band shows a shift to longer wavelength upon elongaton of the thiophene chain, which is quantitatively similar to that observed in absorption. A hint of vibrational structure can be discerned for $\mathbf{HL^2}$ and $\mathbf{HL^3}$, which becomes fully resolved in the spectra recorded at 77 K (∼1400 cm^{-1}). The emission lifetimes are <1 ns at 298 K and around 2 ns at 77 K. Notably, no phosphorescence was observed even at 77 K, suggesting that the rate of intersystem crossing to the triplet state is much slower than the radiative rate of fluorescence.

3. UV−Visible Absorption and Emission Spectroscopy of the Pt(II) Complexes Pt-1, Pt-2, and Pt-3. The absorption spectra of the three platinum complexes are shown in Figure 4. Each complex shows two main sets of bands. The higher energy bands (at around 300, 350, and 375 nm for **Pt-1**, **Pt-2**, and **Pt-3,**

dx.doi.org/10.1021/ic200210e |*Inorg. Chem.* 2011, 50, 3804–3815

Scheme 1. Synthesis of the New Proligands HL^2 and HL^3

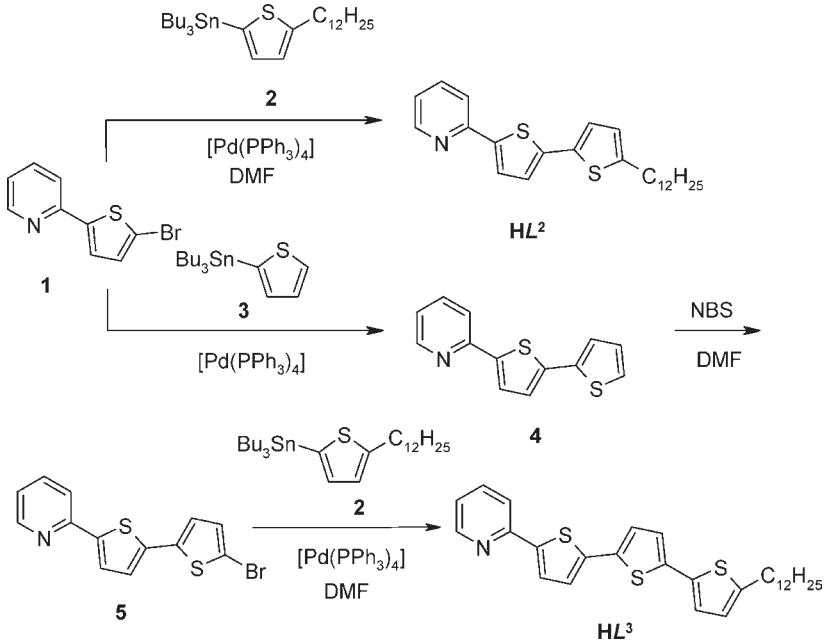

Scheme 2. Synthetic Route to the Pt(II) and Ir(III) Complexes

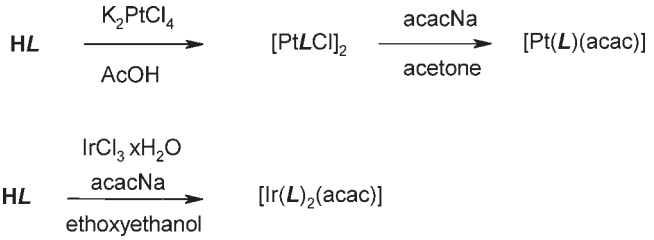

respectively) appear at roughly comparable positions to those of the ligands, suggesting that they arise from ligand-based transitions. Each complex also exhibits a lower-energy band at substantially longer wavelength than the absorption of the ligands, which are likely to arise from charge-transfer transitions involving the metal. The origin of these bands is considered in more detail with the aid of TD-DFT calculations in the subsequent sections. It may be noted here that there is again a trend to longer wavelengths upon elongation of the thiophene chain, as observed in the proligands, with the bands appearing at around 400, 440, and 460 nm for **Pt-1**, **Pt-2**, and **Pt-3** respectively.

Pt-1 displays strong phosphorescence in deaerated solution at room temperature, as reported previously by Thompson and coworkers.[14] The emission spectrum is vibrationally well resolved, with the 0,0 band at 554 nm (Figure 5 and Table 1). No fluorescence is detectable at higher energies. Two independent measurements were made of the phosphorescence lifetime in CH_2Cl_2 using different instrumentation, one using TCSPC upon excitation with a picosecond laser diode source at 374 nm and the other by multichannel scaling with excitation at 420 nm using a xenon microsecond flashlamp. The techniques gave consistent results, but the lifetime of 21 ± 2 μs recorded is surprisingly longer than the value of 4.5 μs previously reported in MeTHF.[14] Our recorded luminescence quantum yield of 0.36 ± 0.1 in CH_2Cl_2 is also substantially higher than the previous report of 0.11 in MeTHF. Though a solvent effect might be suspected, we obtained a similar lifetime of 23 μs in MeTHF, from which we can only conclude that the previously reported values may have been underestimated. We also note a discrepancy between the emission maxima (556 nm in our case in MeTHF, compared to 575 nm in the earlier report in the same solvent). On the other hand, our recorded data are in good agreement with a recent study which included the luminescence maximum, lifetime, and quantum yield (558 nm, 21 μs, and 0.42, respectively) of **Pt-1** in CH_2Cl_2.[22] The highly structured emission spectrum, whose energy is scarcely affected upon cooling to 77 K (Table 1), and the relatively long luminescence lifetime are suggestive of an emissive state with substantial ligand-centered (LC) character, albeit with sufficient metal character to promote the phosphorescence process through the SOC influence of the metal as well as facilitate the S → T ISC and thus eliminate observable ligand-based fluorescence from the singlet state.

The emission spectrum of **Pt-2** is very different from that of **Pt-1** in that it displays *two* sets of bands: a broad, unstructured band around 500 nm and bands >700 nm showing some evidence of vibrational structure (Figure 5). The intensity of both bands is very weak: the total emission quantum yield is around 2 orders of magnitude lower than that of **Pt-1**. The excitation spectra of both the high- and low-energy bands match closely the absorption spectrum of the complex. This observation tends to rule out the possibility that the low-energy band might arise from a dimer or aggregate species, since such emission is typically accompanied by an additional band in the excitation/absorption spectra, as in the case of MMLCT states, for example. Moreover, the relative ratio of the band intensities is independent of concentration in the range investigated (up to 10^{-4} M), ruling out assignment of the low-energy emission to an excimer. The lifetime of the higher-energy emission is <0.5 ns, suggesting that this band is due to spin-allowed fluorescence from the singlet

dx.doi.org/10.1021/ic200210e |*Inorg. Chem.* 2011, 50, 3804–3815

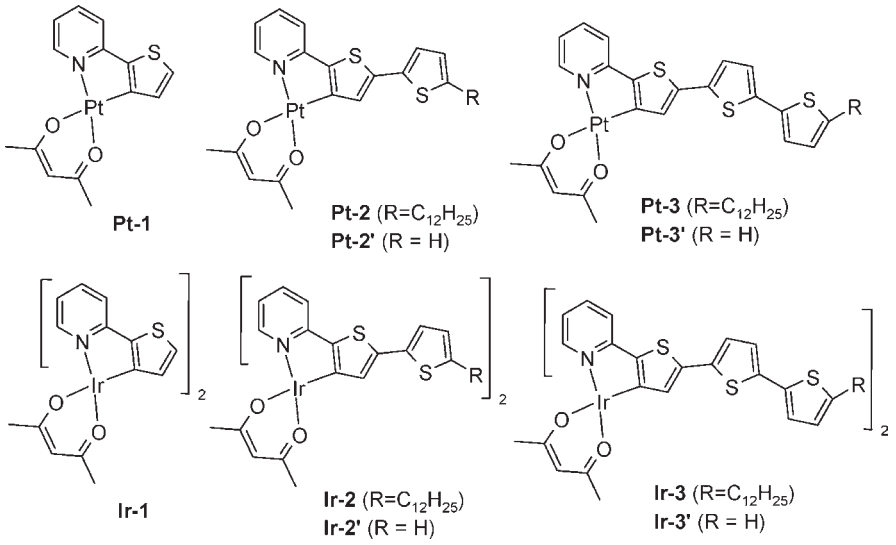

Figure 1. Pt(II) and Ir(III) complexes.

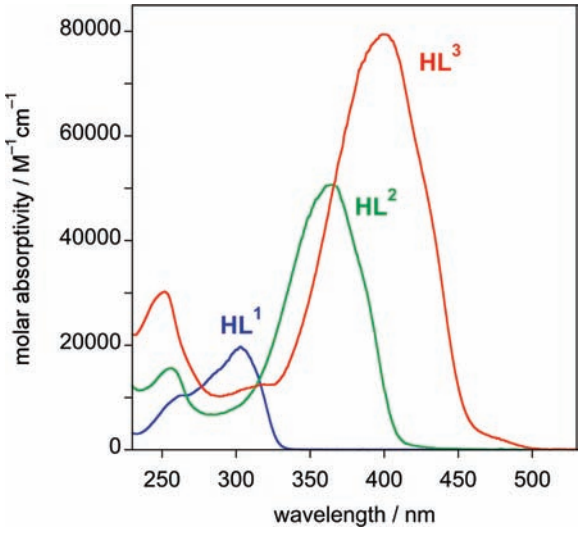

Figure 2. Absorption spectra of HL^1, HL^2, and HL^3 in CH_2Cl_2 at 298 ± 3 K.

state. It is red shifted by around 60 nm compared to the fluorescence of the proligand HL^2. At 77 K, vibrational structure within this band becomes clearly resolved (Figure 5). The intensity distribution of the vibrational components differs for the complex compared to the ligand. The 0,0 band is the most intense for the complex, whereas the 0,1 band is the most intense in the ligand (i.e., the ligand has the larger Huang−Rhys factor), consistent with the higher rigidity expected to be associated with the metal-bound fluorophore compared to the proligand. A reliable value for the lifetime of the lower-energy bands could not be obtained due to the low intensity, compounded by the poor sensitivity of the detector in the NIR region. However, these bands are diminished in intensity in aerated solution, consistent with the expectation that they be due to longer-lived phosphorescence from the triplet state, as observed in **Pt-1**, but substantially red shifted. In summary, **Pt-2** displays dual fluorescence and phosphorescence. Apparently, S → T ISC is not fast enough to completely eliminate the fluorescence, while the triplet state, once formed, emits with much lower efficiency than **Pt-1**, leading to an inferior quantum yield. Both observations would be consistent with a smaller contribution of metal character (and hence SOC) in the pertinent excited states, and we return to this point in section 7. A decrease in ISC with increasing distance of the baricenter of the conjugated system from the metal has been similarly demonstrated in a series of osmium(II) complexes bearing aryl acetonate ligands[11] and in a pair of Pt(II) complexes with acetylide substituted hexa-peri-hexbenzocorone ligands.[9c]

Similar dual emission is observed for **Pt-3** (Figure 5 and Table 1). The bands are red shifted compared to those of **Pt-2**, which reflects the trend observed in the proligands HL^2 and HL^3 and attributable to the more extended π-conjugated structure, although the shift of about 30 nm for both the higher- and lower-energy bands in the complexes is smaller than that observed in the proligands. The intensity of the emission is even weaker than for **Pt-2**.

4. UV−Visible Absorption and Emission Spectroscopy of the Ir(III) Complexes Ir-1, Ir-2, and Ir-3. The photophysical behavior of the iridium complexes is, to a considerable extent, quite comparable to that of the platinum analogues. The absorption spectra again comprise two main sets of bands (Figure 6 and Table 1). The lower-energy bands can again be attributed to charge-transfer transitions, in line with the well-established assignments for cyclometalated iridium complexes with arylpyridine ligands. They appear at lower energies than the corresponding bands in their platinum(II) counterparts but display the same trend to longer wavelengths with extension of the thiophene chain on going from **Ir-1** to **Ir-2** to **Ir-3**.

Ir-1 is strongly luminescent in solution. Its emission spectrum is slightly red shifted compared to that of **Pt-1** (0,0 bands at 564 and 554 nm, respectively), and the vibrational structure is rather less sharp, which would be consistent with a somewhat greater contribution of MLCT character into an otherwise ligand-centered emissive state, Figure 7. In line with this notion is the observation that the luminescence lifetime of 6.3 μs is significantly shorter than that of **Pt-1** (21 μs), suggesting that the metal-mediated SOC pathways facilitating triplet radiative decay are more efficient in the iridium

dx.doi.org/10.1021/ic200210e |*Inorg. Chem.* 2011, 50, 3804–3815

Table 1. Absorption and Emission Data for the Ligands and Their Platinum and Iridium Complexes[a]

					emission 77 K	
	absorption λ_{max} / nm (ε / μ^{-1} cm^{-1})	emission λ_{max} / nm	τ / ns	$\Phi_{lum} \times 10^{2}$[b]	λ_{max}/nm	τ/ns
HL^1	303 (19 700), 263 (10 400)	351		3.2		
HL^2	364 (50 600), 256 (15 600)	434	~0.5	18	407, 430, 456,	2.1
HL^3	400 (79 400), 251 (30 200)	491	<0.5	11	455, 486, 520,	2.4, 0.8 (biexp)
[Pt(L^1)(acac)], **Pt-1**	421 (4640), 403 (5210), 359 (7480), 332 (18 000), 316 (17 300), 286 (17 700)	554, 556, 602, 654	21 000	36	549, 571, 596, 622, 652	23 000
[Pt(L^2)(acac)], **Pt-2**	443 (18 300), 350 (32 600), 295 (16 800)	495 706, 775	<0.5 2300	0.58	470, 505, 538 693, 724, 767	<0.5 not determinable
[Pt(L^3)(acac)], **Pt-3**	458 (29 200), 374 (28 400), 242 (22 500)	525 735	[e] [e]	0.20	497, 532, 568 [d]	[e]
[Ir(L^1)$_2$(acac)], **Ir-1**	463 (6710), 413 (6230), 316 (28 300), 282 (33 500)	564, 606	6300	46	554, 576, 601, 627, 658	10 200
[Ir(L^2)$_2$(acac)], **Ir-2**	482 (13 200), 366 (38 000), 333 (33 100), 272 (29 300)	[b] 704, 775	[c] 1300	0.30	[c] 695, 730, 771	[e] 1200
[Ir(L^3)$_2$(acac)], **Ir-3**	499 (36 100), 418 (83 900), 247 (45 300)	456, 490, 519 793	[e] [e]	0.045	405, 428, 457, 481, 538 782	[e] 1200

[a] In CH_2Cl_2 except for values at 77 K, which are in diethyl ether/isopentane/ethanol (2:2:1 v/v). [b] Where dual emission is observed, the reported values refer to the total emission quantum yields. [c] No significant fluorescence. [d] No clear phosphorescence bands for this complex at 77 K; if present, they are swamped by the fluorescence. [e] Emission intensity too weak to record the lifetime.

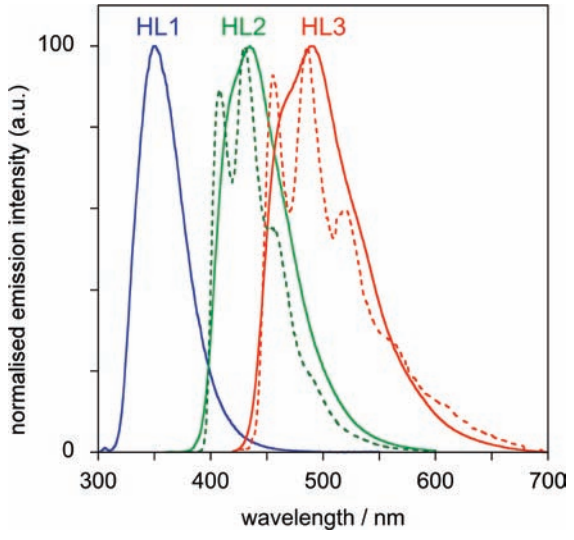

Figure 3. Fluorescence spectra of **HL**^{1}, **HL**^{2}, and **HL**^{3} in CH_2Cl_2 at 298 ± 3 K (solid lines) upon excitation into their lowest-energy absorption bands, and the corresponding spectra at 77 K in a glass of EPA (ether/isopentane/ethanol, 2:2:1 v/v).

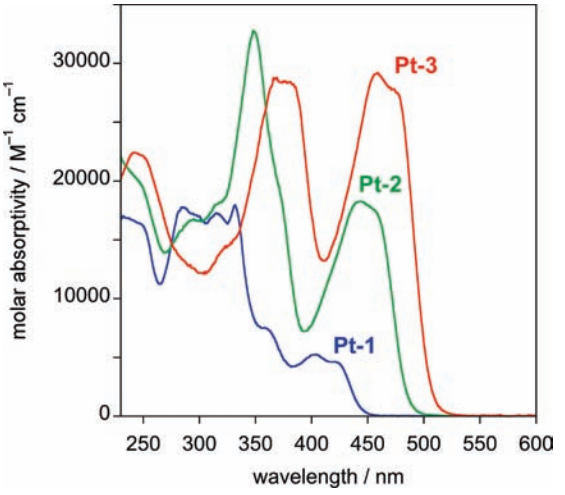

Figure 4. Absorption spectra of **Pt-1**, **Pt-2**, and **Pt-3** in CH_2Cl_2 at 298 ± 3 K.

complex. As for **Pt-1**, no fluorescence is detectable at higher energies.

Ir-2 displays a weaker, red-shifted emission compared to **Ir-1**, emitting in the far red/NIR ($\lambda_{0,0}$ = 704 nm; $\Phi = 0.3 \times 10^{-2}$), with a vibrational spacing similar to that in **Ir-1**, and a lifetime of 1.3 μs. The logical conclusion is that these bands are due to phosphorescence from the triplet state, similar to that displayed by **Pt-2**. In contrast to **Pt-2**, however, there is no evidence of any significant fluorescence at higher energies, suggesting that the S → T ISC process may be more efficient than in the Pt analogue. This conclusion might suggest a greater degree of mixing of metal orbitals into the frontier orbitals involved in the excitations, a point we return to below. The spectrum at 77 K is similar to that at room temperature, but the vibrational structure in the bands becomes more clearly resolved.

The terthiophene complex **Ir-3** displays dual emission. A weak, very low-energy band is observed in the NIR ($\lambda \approx$790 nm). A reliable lifetime could not be obtained at room temperature, but at 77 K, τ = 1.2 μs, consistent with the expected phosphorescent origin and red shift compared to **Ir-2**. In contrast to **Ir-2**, however, **Ir-3** also displays a set of

dx.doi.org/10.1021/ic200210e |*Inorg. Chem.* 2011, 50, 3804–3815

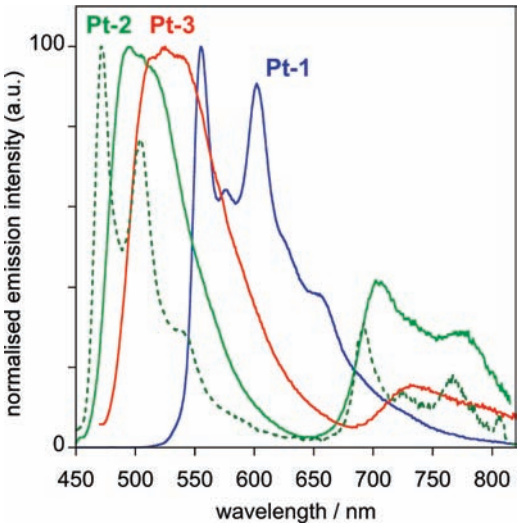

Figure 5. Normalized emission spectra of **Pt-1**, **Pt-2**, and **Pt-3** in CH_2Cl_2 at 298 ± 3 K upon excitation into the lowest-energy absorption band in each case. The emission spectrum of **Pt-2** at 77 K in EPA is also shown (dashed line).

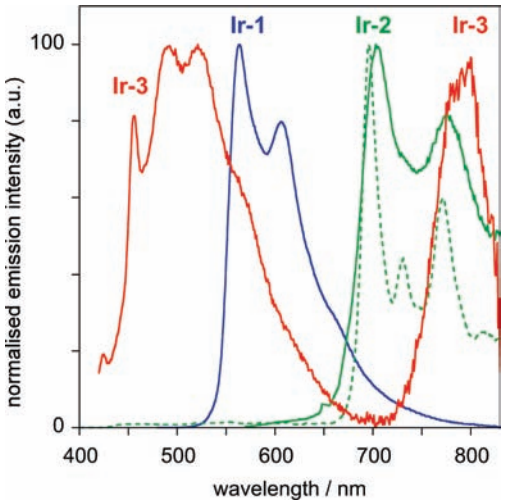

Figure 7. Normalized emission spectra of **Ir-1**, **Ir-2**, and **Ir-3** in CH_2Cl_2 at 298 ± 3 K, and the emission spectrum of **Ir-2** at 77 K in EPA (dashed line). (The sharp, high-energy feature in **Ir-3** is a Raman band of the solvent.)

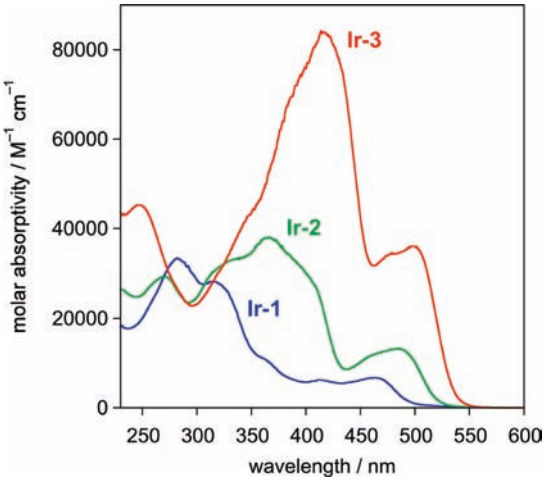

Figure 6. Absorption spectra of **Ir-1**, **Ir-2**, and **Ir-3** in CH_2Cl_2 at 298 ± 3 K.

higher-energy fluorescence bands, similar to the dual emission of **Pt-2** and **Pt-3**.

In summary, all six complexes display phosphorescence. For Pt, the change from one to two thiophenes is accompanied by the appearance of an additional fluorescence band, indicating that the ISC rate is slowed down to a value more comparable to the singlet radiative rate constant, perhaps due to decreasing metal character in the orbitals. In the case of iridium, this change appears only upon going from two to three thiophenes.

5. Computed Geometries. Analogues of the newly obtained Pt complexes, in which the dodecyl chain is replaced by a hydrogen atom (denoted **Pt-2′** and **Pt-3′**), were used as models in the calculations in order to reduce the number of atoms and increase the computational speed. The optimized ground-state geometry structures are shown in Figure 8. Bond lengths and angles at the metal are similar for all three complexes. The calculated ground-state geometrical parameters of **Pt-1** are in good agreement with crystal structural data.[14] The calculated Pt−C bond length of 1.979 Å matches the experimental value. The Pt−N (2.036 Å) and Pt−O bond lengths (2.026−2.123 Å) are 0.03−0.04 Å longer than the measured values. The calculated N−Pt−C1 angle (80.8°) agrees well with experimental data (80.9°), while the O−Pt−O angle (91.3°) is a little smaller than the experimental one (92.3°).[14]

The optimized ground-state geometry structures of the corresponding model iridium complexes are also shown in Figure 8. Since no crystal structure of **Ir-1** has been reported, we compared our calculated ground-state geometry of **Ir-1** with [Ir(thq)$_2$(acac)], where Hthq is 2-thienylquinoline.[23] Complex **Ir-1** possesses C_2 symmetry. Calculated Ir−C bond lengths of 2.004 Å and Ir−O bond lengths of 2.183 Å are overestimated by about 0.01−0.02 Å in comparison with the measured values, whereas the Ir−N bond lengths of 2.087 Å are closer to the experimental values. The calculated N−Ir−C1 angle (80.1°) agrees well with the experimental data (80.1°), while the O−Pt−O angle (85.4°) is smaller than the experimental one (86.4°). Our data are in good agreement with DFT calculations published for **Ir-1** that employed the B3LYP/LANL2DZ basis sets.[24]

6. Molecular Orbitals in the Ground State. *Pt Complexes.* Contour plots of the frontier molecular orbitals of the Pt^{II} complexes in their ground states are shown in Figure 9. The energies and descriptions of the molecular orbitals, in terms of their % composition of ligand and metal orbitals, are collected in Table S1 in the Supporting Information. An energy level diagram of the molecular orbitals is presented in Figure 10. For **Pt-1**, the electron density in the HOMO and HOMO−1 orbitals is delocalized over the thienylpyridine (thpy) and acac ligands and the Pt atom, in which the contributions from metal 5d orbitals are 23% and 29%, respectively (Table 2). There is substantial metal−ligand mixing with the π orbitals of the ligands. HOMO−2 is mainly based on Pt (93% of 5d contribution). The LUMO and LUMO+2 are predominantly localized on the thpy moiety (91%), while LUMO+1 is shared between thpy and acac ligand π^* orbitals (33% and 65%, respectively). Such MO compositions are typical for cyclometalated Pt complexes with β-diketonato auxiliary ligands.[14,25]

dx.doi.org/10.1021/ic200210e |*Inorg. Chem.* 2011, 50, 3804–3815

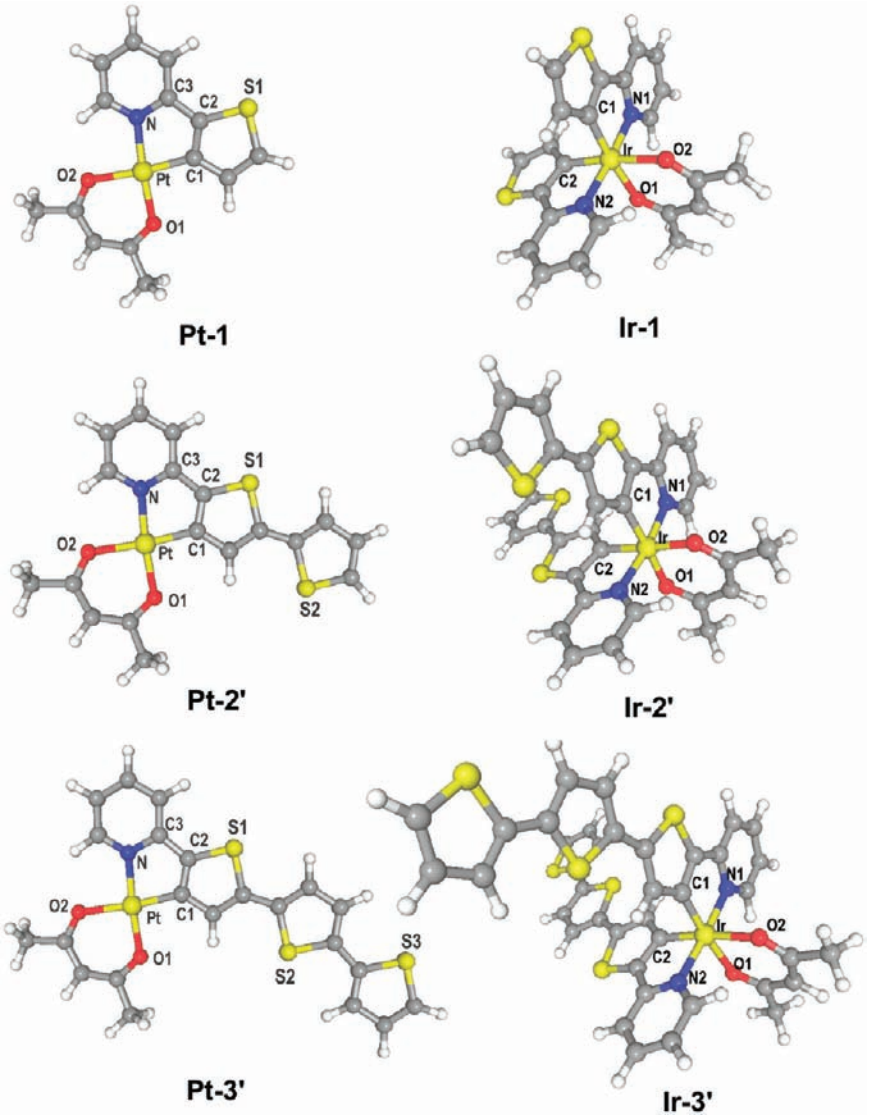

Figure 8. Optimized geometry structures of the Pt and Ir complexes in their ground states.

Extension of the number of thiophene rings in the ligand changes quite dramatically the composition of the highest occupied orbitals in the platinum complexes. In **Pt-2′**, the HOMO is predominantly localized on the thpy ligand (90%) with a low contribution of the metal 5d (9%) (Table 2). Incorporation of the third thiophene ring in **Pt-3** increases the π character of the HOMO up to 95% (only 4% of Pt) and indicates very weak metal−ligand mixing in the HOMOs of **Pt-2′** and **Pt-3′**. The energies of the HOMOs in **Pt-2′** and **Pt-3′** rise significantly compared to that of **Pt-1** (Table 2, Figure 10), while HOMOs−1 (with substantial d character, 30% and 28% of the Pt contribution, respectively, in **Pt-2′** and **Pt-3′**) are less sensitive. Thus, an increase in the π character of the HOMO is also accompanied by increasing the difference between the energies of HOMO and HOMO−1. The LUMOs in **Pt-2′** and **Pt-3′** are localized mainly on the *o*-thpy ligands (95% and 97%). Extension of the conjugation system is thus seen to lead to a clear decrease in the energy gap between HOMO and LUMO (Figure 10).

Ir Complexes. Contour plots of the frontier molecular orbitals in the ground states of the Ir complexes are shown in Figure 11, with energies and descriptions (% contribution of ligand and metal orbitals) collected in Table S2 in the Supporting Information. The electron density in the ground state HOMO of **Ir-1** is localized on the thienylpyridine (thpy) and the Ir atom (36% contribution from metal 5d; see Table 2), indicating substantial mixing of the π orbitals of the ligands with the metal. HOMO−1 and HOMO−2 are near-degenerate (energy difference is 0.17 eV), but they have different character. HOMO−1 has a large contribution from the metal (39% Ir 5d), while HOMO−2 is purely a π orbital mainly based on the thienylpyridines (<3% contribution of 5d). The LUMO and LUMO+1 are degenerate and predominantly localized on the thpy moieties (88% and 86%, respectively), i.e., ligand π^* orbitals. Similar MO compositions have been calculated for **Ir-1** by DFT using the B3LYP/LANL2DZ level.[26]

As in the platinum complexes, extension of the oligothiophene chain substantially changes the composition of the highest-occupied molecular orbitals in the iridium complexes too. Although the energies of the HOMOs in **Ir-2′** and **Ir-3′** are not significantly changed compared with **Ir-1** (differences < 0.15 eV), the

dx.doi.org/10.1021/ic200210e |*Inorg. Chem.* 2011, 50, 3804–3815

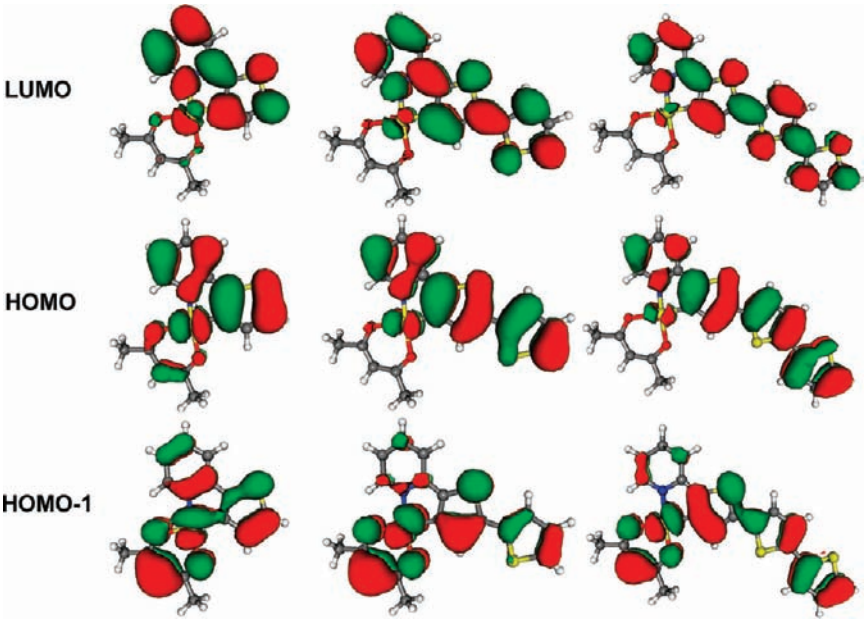

Figure 9. Contour plots of the frontier molecular orbitals in the ground state of **Pt-1** (left), **Pt-2′** (center), and **Pt-3′** (right).

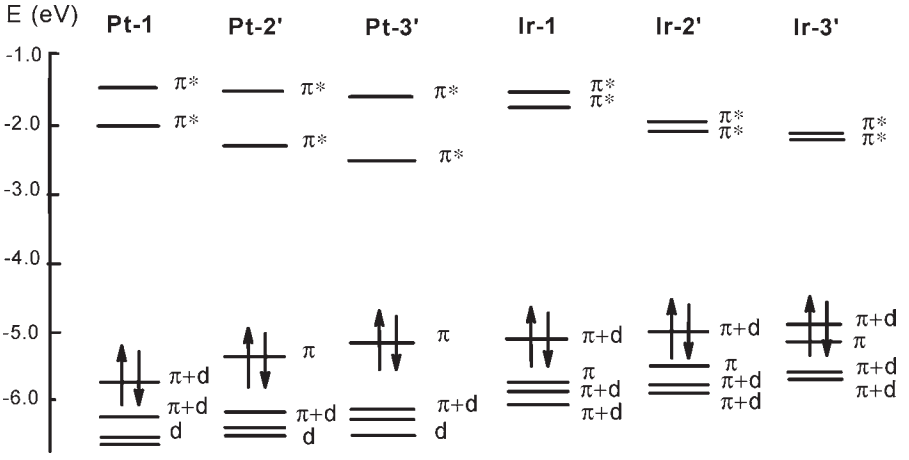

Figure 10. Energy level diagram of the molecular orbitals of the complexes.

Table 2. Calculated Contribution of the Metal in Frontier Molecular Orbitals in the Ground States of the Complexes

	contribution of the metal in MO (%)			
	HOMO−2	HOMO−1	HOMO	LUMO
Pt-1	92.4	29.4	23.3	7.0
Pt-2′	42.9	29.7	8.8	4.2
Pt-3′	33.7	27.9	4.2	2.5
Ir-1	2.7	39.2	36.2	4.1
Ir-2′	39.2	3.4	25.1	2.8
Ir-3′	27.8	0.8	16.6	1.5

contributions of metal d orbitals in **Ir-2** and **Ir-3** are significantly lower (25% and 16%, respectively). The extension of the conjugated system increases significantly the energy of the thpy-localized HOMO−1 orbitals up to −5.41 and −5.18 eV for **Ir-2′** and **Ir-3′**, respectively (Figure 10), such that they have essentially pure π character (only 3% and 1% of Ir contribution) and lie close to the HOMO. Indeed, in **Ir-3′**, HOMO (πd character) and HOMO−1 (π character) are almost degenerate. Degenerate LUMOs and LUMOs+1 in **Ir-2′** and **Ir-3′** are localized mainly on the *o*-thpy ligands (95% and 97%). As for Pt, the extension of the conjugation leads to a significant decrease in the energy gap between HOMO and LUMO.

7. Excitation Energies. *Platinum Complexes.* The results from TD-DFT calculations for **Pt-1**, **Pt-2′**, and **Pt-3′** at optimized ground-state geometries are shown in Table S3 in the Supporting Information. For each complex, we typically give the vertical excitation energies for the lowest 10 singlet and 3 triplet states calculated at the optimized structure for the ground state. The orbitals involved in the dominant excitation process are also shown. Energy levels of the lowest singlet and triplet excited states are shown in Figure 12. For **Pt-1**, excitation to the lowest triplet state T_1 (energy = 2.42 eV) occurs from the HOMO with

dx.doi.org/10.1021/ic200210e |*Inorg. Chem.* 2011, 50, 3804–3815

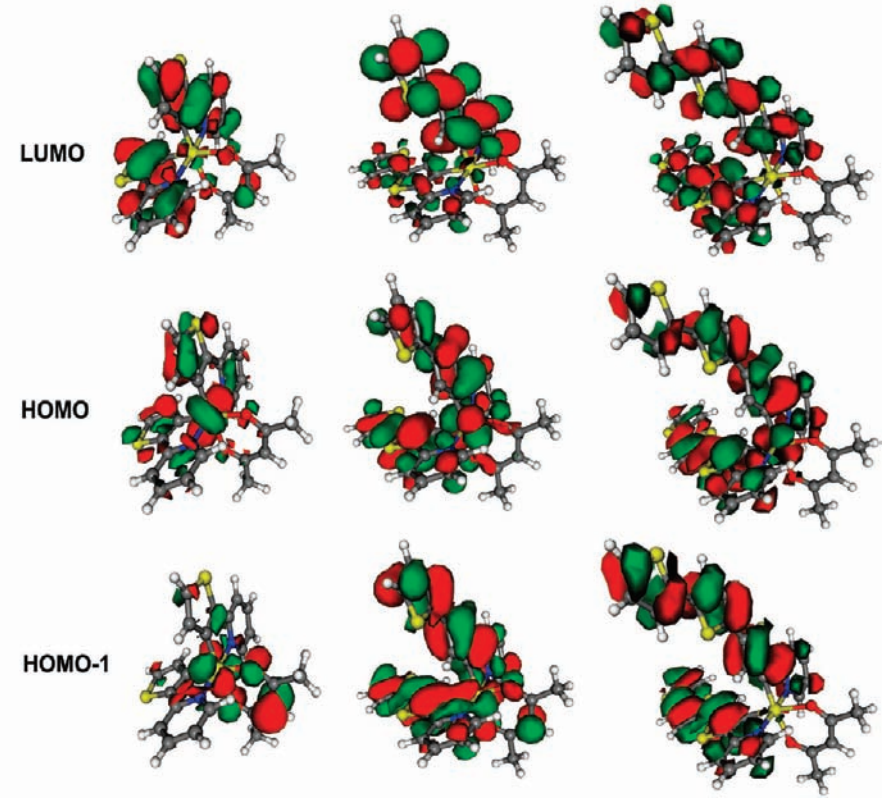

Figure 11. Contour plots of frontier orbitals in the ground state for **Ir-1** (left), **Ir-2′** (center), and **Ir-3′** (right).

πd character to the LUMO with π^* character. The corresponding singlet state S_1 is about 0.67 eV higher at 3.09 eV. The calculated $S_0 \rightarrow S_1$ absorption is in quite good agreement with the experimental value (difference of 20 nm), which lends confidence to the calculations and supports the assignment of the lowest excited states as being of mixed MLCT and ligand-centered $\pi\pi^*$ (LC) character, as previously described.[14]

For **Pt-2′**, the energy of the lowest singlet excited state is 0.23 eV lower than in **Pt-1**, while the difference between the lowest-energy triplet states is more substantial at 0.52 eV. The lowest-energy transitions are again from HOMO to LUMO, as in **Pt-1**. However, because of the low contribution of Pt d orbitals in HOMO, we would label the lowest excited state in **Pt-2′** as $\pi\pi^*$ (LC), not MLCT or mixed MLCT/LC. Extension of the conjugation system in **Pt-3′** results in a significant decrease in the S_1 and T_1 excited state energies (by 0.43 and 0.75 eV, respectively), which can also be designated as $\pi\pi^*$ because of the very low contribution of the metal in HOMO and LUMO involved in the lowest energy excitations. Calculated absorption spectra of Pt complexes are shown in Figure 13.

Iridium Complexes. The results from TD-DFT calculations for **Ir-1**, **Ir-2′**, and **Ir-3′** are shown in Table S4 in the Supporting Information, where the lowest 10 singlet and 3 triplet states calculated at the optimized geometry of the ground state are given. Energy levels of the lowest singlet and triplet excited states are shown in Figure 14. Calculated absorption spectra of Ir complexes are shown in Figure 15. In **Ir-1**, excitation to the lowest triplet state T_1 (energy = 2.34 eV) can be designated as a mixed $\pi\pi^*$/MLCT state from inspection of the orbitals involved in the transition (HOMO → LUMO). The corresponding singlet state S_1 is about 0.67 eV higher at 2.76 eV, also having mixed $\pi\pi^*$/MLCT character, as concluded from previous calculations.[23]

Extension of the oligothophene chain leads to a significant decrease of the lowest excited states in **Ir-2′** and **Ir-3′** compared with those of **Ir-1**. The lowest energy transitions in **Ir-2′** and **Ir-3′** occur from HOMO to LUMO. The low contribution of the metal in the frontier orbitals results in substantial decreasing of MLCT character of these transitions, approaching toward essentially pure $\pi\pi^*$ character at **Ir-3′**.

8. Discussion. The presence of a heavy atom, such as platinum or iridium, is anticipated to increase spin−orbit coupling and thus intersystem crossing, provided that its orbitals participate signficantly in the excited states involved. In small, cyclometalated Pt(II) and Ir(III) complexes, this is typically the case, and population of the triplet state from the singlet is favored to such an extent that fluorescence cannot compete with ISC ($k_{ISC} \gg k_f$) and no fluorescence is observed. This is the case for **Pt-1** and **Ir-1**. The much lower participation of the metal d orbitals in the HOMO in **Pt-2** and **Pt-3** will render metal−ligand mixing into the lowest excited states much less efficient, such that the influence of spin−orbit coupling associated with the heavy atom will be attenuated. Thus, one may anticipate that the rate of $S_1 \rightarrow T_1$ ISC will be reduced, allowing the $S_1 \rightarrow S_0$ radiative process to compete and fluorescence to be observable ($k_{ISC} \approx k_f$). This explains the observation of fluorescence in addition to phosphorescence in **Pt-2** and **Pt-3**. The increasing energy gap between the S_1 and the T_1 states will also lead to a reduction in the $S_1 \rightarrow T_1$ rate due to a poorer overlap integral, compounding the above effect. Moreover, the inefficient SOC will also mean that the rate of the formally forbidden radiative $T_1 \rightarrow S_0$ process will not be

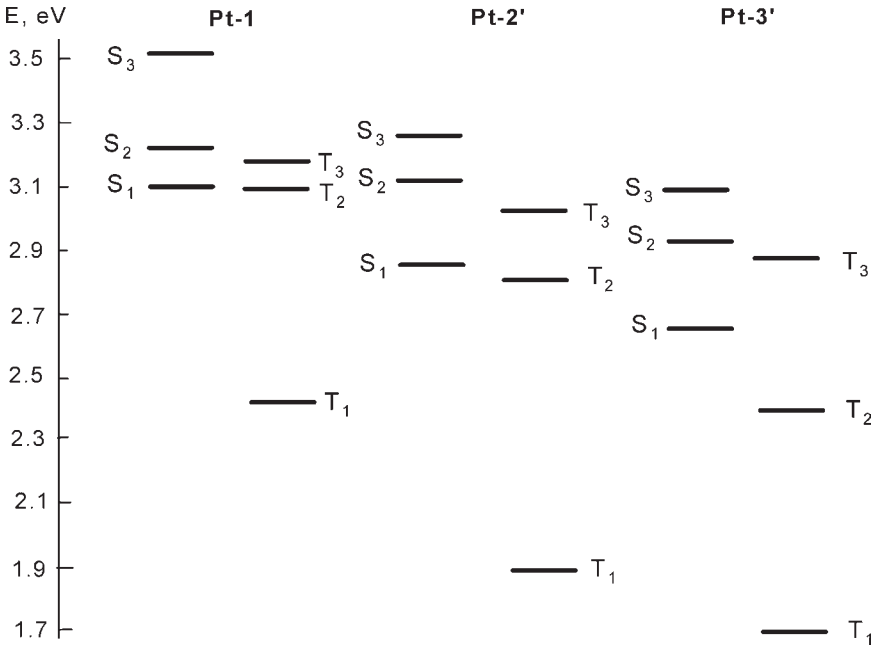

Figure 12. Energy level diagram of the lowest energy excited states of Pt complexes.

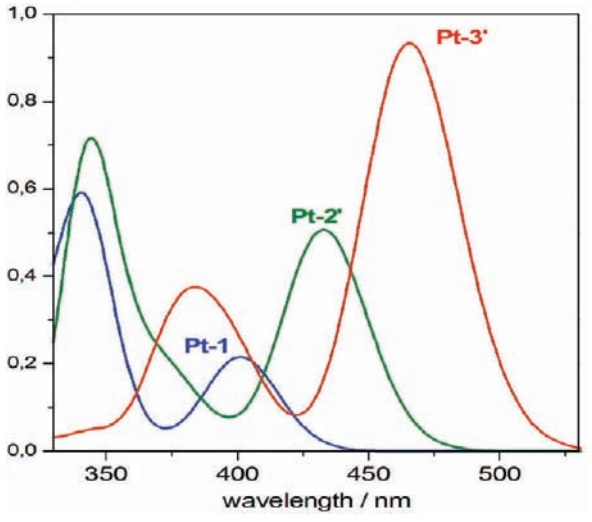

Figure 13. Simulated absorption spectra of Pt complexes from TD-DFT.

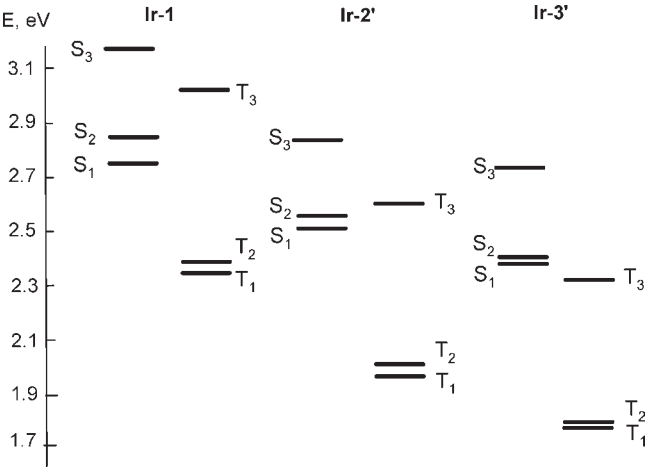

Figure 14. Energy level diagram of the lowest energy excited states of Ir complexes calculated by TD-DFT.

facilitated to the same extent as it was in **Pt-1**. This is probably a key reason why the phosphorescence quantum yields of **Pt-2** and **Pt-3** are so low compared to **Pt-1**. Nonradiative decay is also expected to be increased as the emission energy of **Pt-2** and **Pt-3** is substantially lower than **Pt-1**, in line with the energy gap law.

A somewhat similar trend is observed for the iridium complexes. However, in this case, there is still sufficient metal character in the S_1 state of **Ir-2** (in contrast to **Pt-2**) to ensure that the $S_1 \rightarrow T_1$ process is still much faster than the rate of $S_1 \rightarrow S_0$, and no fluorescence is observed. Note that the TD-DFT calculations designated the S_1 state as mixed $\pi\pi^*$/MLCT in **Ir-2** but $\pi\pi^*$ in **Pt-2** (Tables S4 and S3, respectively, in the Supporting Information). When **Ir-3** is reached, it too has a $\pi\pi^*$-based S_1 state (Table S4 in the Supporting Information), and indeed, a fluorescence band appears in the emission spectrum of this complex too.

Comparison of Figure 13 with Figure 4 reveals quite a good match between the trends in the calculated and observed absorption spectra of the platinum complexes. The observed red shift with extended conjugation is consistent with the decreasing HOMO−LUMO gap calculated. Moreover, as noted in section 7, the calculations indicate that the triplet state energy drops more rapidly than the singlet state upon introduction of a second thiophene ring onto the thpy ligand, and this is reflected in the larger influence on the phosphorescence energy (Figure 5 and Table 1) than on the energy of the lowest-energy absorption band (Figure 4 and Table 1). Analogous observations are made for the iridum(III) complexes (Figures 6 and 7).

dx.doi.org/10.1021/ic200210e |*Inorg. Chem.* 2011, 50, 3804–3815

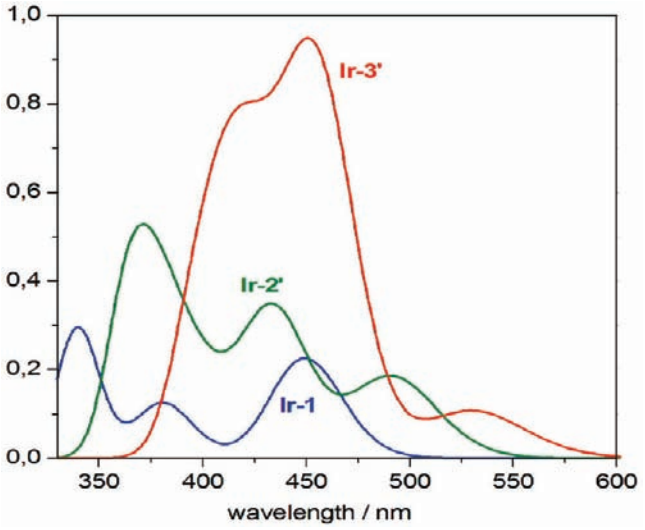

Figure 15. Simulated absorption spectra of Ir complexes from TD-DFT.

CONCLUSION

Cyclometalated metal complexes have become central to the field of the photophysics and photochemistry of coordination complexes and to their application in contemporary technology. The present, systematic study shows that as the size of the conjugated system of the ligand increases, the extent of participation of metal d orbitals in the highest-occupied molecular orbitals decreases. As a result, the influence of the spin−orbit coupling of the metal in promoting both intersystem crossing, $S_1 \rightarrow T_1$, and triplet radiative decay, $T_1 \rightarrow S_0$, is attenuated. An increasing S_1-T_1 energy gap as conjugation increases also has the effect of reducing the rate of intersystem crossing. The consequence is that fluorescence becomes observable while the intensity of the phosphorescence decreases due to the combined effects of a lower yield of triplet formation, a decreased $T_1 \rightarrow S_0$ radiative decay rate, and increased nonradiative decay as the excited state energy decreases. Clearly, the approach of simply extending the conjugation in order to obtain more red-shifted emission starts to break down, a conclusion of particular significance to the design of technologically relevant NIR-emitting complexes.

It can be predicted that for some complexes dual luminescence will be observed, i.e., when the contribution of metal character is still sufficient to promote phosphorescence but not enough for the ultrafast depletion of the singlet state that normally occurs for complexes with discrete arylpyridine ligands. Such conclusions are likely to be quite general, including for metals other than Pt(II) and Ir(III), but the point at which dual emission is observed may be dependent on the metal ion (as in the present case of **Pt-2** compared to **Ir-2**), according to the efficacy of the SOC pathways. The current results reinforce the theory that for metals with similar SOC constants such pathways should be more efficient for octahedral d^6 complexes than for square-planar d^8 complexes.[7]

EXPERIMENTAL SECTION

I. Synthesis. *Typical Procedure for the Stille Coupling.* A mixture of 2-bromothienylpyridine **1** or **5** (5.46 mmol), corresponding tributyltinthiophene **2** or **3** (6.00 mmol), and $[Pd(PPh_3)_4]$ (0.1 mmol) in dry DMF (35 mL) was deaerated by bubbling argon through the mixture, and then the reaction mixture was stirred for 1 h at 115 °C. The solvent was removed under reduced pressure, and the residue was recrystallized from petrol ether or DMF. Full synthetic details and characterization are provided in the Supporting Information.

Preparation of [PtL^n(acac)] Complexes. A solution of K_2PtCl_4 (208 mg, 0.5 mmol) in water (1 mL) was added to a stirred solution of HL^n (0.5 mmol) in acetic acid (30 mL). The mixture was heated at reflux under nitrogen for 15 h. A precipitated solid of Pt(II) μ-dichloro-bridged dimer was filtered off, washed with acetic acid (5 mL) and ethanol (5 mL), and dried in vacuum. The dimer and sodium acetylacetonate (10 equiv) were heated under reflux in acetone for 16 h. The solvent was removed under reduced pressure, and the complex was purified by flash chromatography (silica gel, DCM eluant). Data for [PtL^1(acac)] (**Pt-1**) was consistent with that previously reported.[13] Full details of the synthesis and characterization of **Pt-2** and **Pt-3** are provided in the Supporting Information.

Preparation of [Ir(L^n)$_2$(acac)] Complexes. The ligand HL^n (0.2 mmol), $IrCl_3 \cdot xH_2O$ (Ir 55% min, 35 mg, 0.1 mmol), and sodium acetylacetonate (140 mg, 1 mmol) in a mixture of ethoxyethanol (30 mL) and water (10 mL) were heated under reflux under nitrogen for 15 h. The solvent was then removed under reduced pressure, and the residue was purified by flash chromatography (silica gel, DCM eluant). Data for [Ir(L^1)$_2$(acac)] (**Ir-1**) were consistent with those previously reported.[27] Full details of the synthesis and characterization of **Ir-2** and **Ir-3** are provided in the Supporting Information.

ii. Instrumentation for Optical Spectroscopy. Absorption spectra were measured on a Biotek Instruments XS spectrometer using quartz cuvettes of 1 cm path length. Steady-state luminescence spectra were measured using a Jobin Yvon FluoroMax-2 spectrofluorimeter, fitted with a red-sensitive Hamamatsu R928 photomultiplier tube; the spectra shown are corrected for the wavelength dependence of the detector, and the quoted emission maxima refer to the values after correction. Degassing was achieved via a minimum of three freeze−pump−thaw cycles while connected to the vacuum manifold; the final vapor pressure at 77 K was $<5 \times 10^{-2}$ mbar, as monitored using a Pirani gauge. Luminescence quantum yields were determined using $[Ru(bpy)_3]Cl_2$ in degassed aqueous solution as the standard, for which $\Phi_{lum} = 0.042$;[28] estimated uncertainty in Φ_{lum} is ±20% or better. The luminescence lifetimes of the complexes were measured by time-correlated single-photon counting (TCSPC), following excitation at 374.0 nm with an EPL-375 pulsed-diode laser. The emitted light was detected at 90° using a Peltier-cooled R928 PMT after passage through a monochromator. The estimated uncertainty in the quoted lifetimes is ±10% or better. For **Pt-1**, the lifetimes at both 298 and 77 K were independently measured by multichannel scaling using a xenon microsecond flashlamp as the excitation source in conjunction with an R928 detector.

iii. Computational Methods. For all calculations, the Orca 2.8.0 package of programs was used.[29] In the TD-DFT calculations the B3LYP hybrid functional[30,31] was applied. The metals were described by the Stuttgart−Dresden[32] effective core potential (treating the valence electrons explicitly) using the Ahlrichs def2-TZVP[33] basis set of triple-ζ quality. The ground state geometries of the complexes were fully optimized without symmetry constraints at the DFT/B3LYP level using the Ahlrichs double-ζ basis set (VDZ)[34] with polarization functions on all atoms. To investigate the vertical excitation energies of the low-lying excited states of the complexes, TD-DFT calculations were performed using the B3LYP functional together with the Ahlrichs triple-ζ basis set with polarization functions on all atoms (TZVP) at the optimized ground-state (S_0) geometry. The COSMO solvation model[35] was used to calculate the solvent effect in DCM ($\varepsilon = 9.08$, $n_D = 1.424$). To accelerate TD-DFT calculations we employed the RIJCOSX approximation combining the RI-J method and the COSX approximation.[36]

ASSOCIATED CONTENT

Supporting Information. Experimental and computational details and spectral characterization data for new compounds,

dx.doi.org/10.1021/ic200210e |*Inorg. Chem.* 2011, 50, 3804–3815

calculated molecular orbital compositions in the ground states (Tables S1 and S2), excited energies, dominant orbital excitations, and oscillator strength (f) from TD-DFT calculations (Tables S3 and S4) for the Pt(II) and Ir(III) complexes. This material is available free of charge via the Internet at http://pubs.acs.org.

AUTHOR INFORMATION

Corresponding Author

*E-mail: dnk@ios.uran.ru (D.N.K.), duncan.bruce@york.ac.uk (D.W.B), j.a.g.williams@durham.ac.uk (J.A.G.W.).

ACKNOWLEDGMENT

This work was partly supported by the Russian Foundation for Basic Researches. D.N.K. and D.W.B. are grateful to The Royal Society for a Joint Project Grant. We are grateful to Johnson Matthey for a generous loan of K_2PtCl_4.

REFERENCES

(1) (a) Flamigni, L.; Barbieri, A.; Sabatini, C.; Ventura, B.; Barigelletti, F. *Top. Curr. Chem.* **2007**, *281*, 143–203. (b) Lowry, M. S.; Bernhard, S. *Chem.—Eur. J.* **2006**, *12*, 7970–7977. (c) Chi, Y.; Chou, P.-T. *Chem. Soc. Rev.* **2010**, *39*, 638–655. (d) Williams, J. A. G.; Wilkinson, A. J.; Whittle, V. L. *Dalton Trans.* **2008**, 2081–2099. (e) Zhao, Q.; Li, F.; Huang, C. *Chem. Soc. Rev.* **2010**, *39*, 3007–3030.

(2) (a) Williams, J. A. G. *Top. Curr. Chem.* **2007**, *281*, 205–268. (b) Castellano, F. N.; Pomestchenko, I. E.; Shikhova, E.; Hua, F.; Muro, M. L.; Rajapakse, N. *Coord. Chem. Rev.* **2006**, *250*, 1819–1828. (c) Lai, S. W.; Che, C. M. *Top. Curr. Chem.* **2004**, *241*, 27–63.

(3) (a) Nocera, D. G. *Acc. Chem. Res.* **1995**, *28*, 209–217. (b) Doherty, M. D.; Grills, D. C.; Muckerman, J. T.; Polyansky, D. E.; Fujita, E. *Coord. Chem. Rev.* **2010**, *254*, 2472–2482. (c) Cline, E. D.; Bernhard, S. *Chimia* **2009**, *63*, 709–713. (d) Xu, Q. Q.; Fu, W. F.; Zhang, G.-J.; Bian, Z.-Y.; Zhang, J.-F.; Han, X.; Xu, W.-Z. *Catal. Commun.* **2008**, *10*, 49–52.

(4) (a) Chakraborty, S.; Wadas, T. J.; Hester, H.; Schmehl, R.; Eisenberg, R. *Inorg. Chem.* **2005**, *44*, 6865–6878. (b) Hissler, M.; McGarrah, J. E.; Connick, W. B.; Geiger, D. K.; Cummings, S. D.; Eisenberg, R. *Coord. Chem. Rev.* **2000**, *208*, 115–137. (c) Baranoff, E.; Yum, J.-H.; Jung, I.; Vulcano, R.; Grätzel, M.; Nazeeruddin, M. K. *Chem. Asian J.* **2010**, *5*, 496–499.

(5) (a) Lo, K. K.-W. *Top. Organomet. Chem.* **2010**, *29*, 115–158. (b) Fernandez-Moreira, V.; Thorp-Greenwood, F. L.; Coogan, M. P. *Chem. Commun.* **2010**, *46*, 186–202. (c) Murphy, L.; Congreve, A.; Palsson, L. O.; Williams, J. A. G. *Chem. Commun.* **2010**, *46*, 8743–8745. (d) Botchway, S. W.; Charnley, M.; Haycock, J. W.; Parker, A. W.; Rochester, D. L.; Weinstein, J. A.; Williams, J. A. G. *Proc. Natl. Acad. Sci. U.S.A.* **2008**, *105*, 16071–16076. (e) Koo, C. K.; Wong, K. L.; Man, C. W.-Y.; Lam, Y. W.; So, K. Y.; Tam, H. L.; Tsao, S. W.; Cheah, K. W.; Lau, K. C.; Yang, Y. Y.; Chen, J. C.; Lam, M. H.-W. *Inorg. Chem.* **2009**, *48*, 872–878.

(6) In *Highly Efficient OLEDs with Phosphorescent Materials*; Yersin, H., Ed.; Wiley-VCH: Berlin, 2007.

(7) Rausch, A. F.; Homeier, H. H. H.; Yersin, H. *Top. Organomet. Chem.* **2010**, *29*, 193–235.

(8) Danilov, E. O.; Pomestchenko, I. E.; Kinayyigit, S.; Gentili, P. L.; Hissler, M.; Ziessel, R.; Castellano, F. N. *J. Phys. Chem. A* **2005**, *109*, 2465–2471.

(9) (a) Ley, K. D.; Schanze, K. S. *Coord. Chem. Rev.* **1998**, *171*, 287–307. (b) Salassa, L.; Garino, C.; Albertino, A.; Volpi, G.; Nervi, C.; Gobetto, R.; Hardcastle, K. I. *Organometallics* **2008**, *27*, 1427–1435. (c) Kim, K.-Y.; Liu, S.; Köse, M. E.; Schanze, K. S. *Inorg. Chem.* **2006**, *45*, 2509–2519. (d) Chi, Y.; Chou, P.-T. *Chem. Soc. Rev.* **2007**, *36*, 1421–1431.

(10) Leslie, W.; Batsanov, A. S.; Howard, J. A. K.; Williams, J. A. G. *Dalton Trans.* **2004**, 623–631.

(11) (a) Chen, Y.-L.; Li, S.-W.; Chi, Y.; Cheng, Y.-M.; Pu, S.-C.; Yeh, Y.-S.; Chou, P.-T. *ChemPhysChem* **2005**, *6*, 2012–2017.(b) Chou, P.-T.; Chi, Y.; Chung, M.-W.; Lin, C.-C. *Coord. Chem. Rev.* **2011**; DOI: 10.1016/J.CCR.2010.12.013

(12) (a) Wong, W.-Y.; He, Z.; So, S.-K.; Tong, K. L.; Li, Z. *Organometallics* **2005**, *24*, 4079–4082. (b) He, Z.; Wong, W.-Y.; Yu, X.; Kwok, H.-S.; Lin, Z. *Inorg. Chem.* **2006**, *45*, 10922–10937.

(13) Grushin, V. V.; Herron, N.; LeCloux, D. D.; Marshall, W. J.; Petrov, V. A.; Wang, Y. *Chem. Commun.* **2001**, 1494–1495.

(14) Brooks, J.; Babayan, Y.; Lamansky, S.; Djurovich, P. I.; Tsyba, I.; Bau, R.; Thompson, M. E. *Inorg. Chem.* **2002**, *41*, 3055–3066.

(15) (a) Balashev, K. P.; Puzyk, M. V.; Kotlyar, V. S.; Kulikova, M. V. *Coord. Chem. Rev.* **1997**, *159*, 109–120. (b) Yin, B. L.; Niemeyer, F.; Williams, J. A. G.; Jiang, J.; Boucekkine, A.; Toupet, L.; Le Bozec, H.; Guerchais, V. *Inorg. Chem.* **2006**, *45*, 8584–8596. (c) Niedermair, F.; Kwon, O.; Zojer, K.; Kappaun, S.; Trimmel, G.; Mereitere, K.; Slugovc, C. *Dalton Trans.* **2008**, 4006–4014. (d) Ghedini, M.; Pugliese, T.; La Deda, M.; Godbert, N.; Aiello, I.; Amati, M.; Belviso, S.; Lelj, F.; Accorsi, G.; Barigelletti, F. *Dalton Trans.* **2008**, 4303–4318. (e) Wong, W.-Y.; Ho, C.-L. *J. Mater. Chem.* **2009**, *19*, 4457–4482. (f) Liu, J.; Yang, C.-J.; Cao, Q.-Y.; Xu, M.; Wang, H.-N.; Peng, J.; Tan, W.-F.; Lue, X.-X.; Gao, X.-C. *Inorg. Chim. Acta* **2009**, *362*, 575–579. (g) Santoro, A.; Whitwood, A. C.; Williams, J. A. G.; Kozhevnikov, V. N.; Bruce, D. W. *Chem. Mater.* **2009**, *21*, 3871–3882. (h) Feng, K.; Zuniga, C.; Zhang, Y.-D.; Kim, D.; Barlow, S.; Marder, S. R.; Brédas, J. L.; Weck, M. *Macromolecules* **2009**, *42*, 6855–6864. (i) Vezzu, D. A. K.; Deaton, J. C.; Jones, J. S.; Bartolotti, L.; Harris, C. F.; Marchetti, A. P.; Kondakova, M.; Pike, R. D.; Huo, S. *Inorg. Chem.* **2010**, *49*, 5107–5119.

(16) (a) Williams, J. A. G.; Develay, S.; Rochester, D. L.; Murphy, L. *Coord. Chem. Rev.* **2008**, *252*, 2596–2611. (b) Wilkinson, A. J.; Puschmann, H.; Howard, J. A. K.; Foster, C. E.; Williams, J. A. G. *Inorg. Chem.* **2006**, *45*, 8685–8699.

(17) Baldo, M. A.; Lamansky, S.; Burrows, P. E.; Thompson, M. E.; Forrest, S. R. *Appl. Phys. Lett.* **1999**, *75*, 4–6.

(18) Holmes, R. J.; Forrest, S. R.; Tung, Y. J.; Kwong, R. C.; Brown, J. J.; Garon, S.; Thompson, M. E. *Appl. Phys. Lett.* **2003**, *82*, 2422–2424.

(19) Li, C. L.; Su, Y. J.; Chou, P. T.; Chien, C. H.; Cheng, C. C.; Liu, R. S. *Adv. Funct. Mater.* **2005**, *15*, 387–395.

(20) Roncali, J. *Chem. Rev.* **1997**, *97*, 173–205.

(21) McQuade, D. T.; Pullen, A. E.; Swager, T. M. *Chem. Rev.* **2000**, *100*, 2537–2574.

(22) Kozhevnikov, D. N.; Kozhevnikov, V. N.; Ustinova, M. M.; Santoro, A.; Bruce, D. W.; Koenig, B.; Czerwieniec, R.; Fischer, T.; Zabel, M.; Yersin, H. *Inorg. Chem.* **2009**, *48*, 4179–4189.

(23) Zhao, Q.; Jiang, C.-Y.; Shi, M.; Li, F.-Y.; Yi, T.; Cao, Y.; Huang, C.-H. *Organometallics* **2006**, *25*, 3631–3638.

(24) Liu, T.; Xia, B.-H.; Zhou, X.; Zhang, H.-X.; Pan, Q.-J.; Gao, J.-S. *Organometallics* **2007**, *26*, 143–149.

(25) Ma, B.; Djurovich, P. I.; Yousufuddin, M.; Bau, R.; Thompson, M. E. *J. Phys. Chem. C* **2008**, *112*, 8022–8031.

(26) Hay, P. J. *J. Phys. Chem. A* **2002**, *106*, 1634–1641.

(27) Lamansky, S.; Djurovich, P.; Murphy, D.; Abdel-Razzaq, F.; Lee, H.-E.; Adachi, C.; Burrows, P. E.; Forrest, S. R.; Thompson, M. E. *J. Am. Chem. Soc.* **2001**, *123*, 4304–4312.

(28) Van Houten, J.; Watts, R. J. *J. Am. Chem. Soc.* **1976**, *98*, 4853–4858.

(29) Neese, F. et al. . *Orca 2.8.0*; Universität Bonn: Bonn, 2010.

(30) Becke, A. D. *J. Chem. Phys.* **1993**, *98*, 5648–5652.

(31) Lee, C.; Yang, W.; Parr, R. G. *Phys. Rev. B* **1988**, *37*, 785–789.

(32) Andrae, D.; Haeussermann, U.; Dolg, M.; Stoll, H.; Preuss, H. *Theor. Chim. Acta* **1990**, *77* (2), 123–141.

(33) Weigend, F.; Ahlrichs, R. *Phys. Chem. Chem. Phys.* **2005**, *7*, 3297–3305.

(34) Schaefer, A.; Horn, H.; Ahlrichs, R. *J. Chem. Phys.* **1992**, *97*, 2571–2577.

(35) Klamt, A.; Schüürmann, G. *J. Chem. Soc., Perkin Trans. 2* **1993**, 799–806.

(36) Neese, F.; Wennmohs, F.; Hansen, A.; Becker, U. *Chem. Phys.* **2009**, *356*, 98–109.